Simulated Radiance Patterns for Finite Cubic Clouds

THOMAS MCKEE AND STEPHEN K. COX

Department of Atmospheric Science, Colorado State University, Fort Collins 80523

(Manuscript received 11 December 1975, in revised form 28 June 1976)

ABSTRACT

Calculated distributions of scattered shortwave radiance are presented for simulated cumulus clouds using a cubic shape. Comparison with similar clouds of semi-infinite horizontal extent is included. For an incident solar zenith angle of 0° the angular distribution of the radiance exiting the cloud top is similar for the cube and the semi-infinite layer, but the radiance from the cube is much smaller for optical depths between 9.8 and 73.5. At an optical depth of 73.5 the vertical radiance from the cube is only 58% of the radiance from the semi-infinite layer cloud. For an incident solar zenith angle of 60°, the angular distribution and the magnitudes of the scattered radiances are similar for the cube top and the semi-infinite layer. A comparison of the total radiance from the cube top and side in the solar plane shows a dramatic change in angular distribution compared with the semi-infinite cloud. Radiances exiting the antisolar side of the cube illustrate the strong forward scattering for short optical paths near cloud edges. The transition from cubic clouds to semi-infinite layers is illustrated for a vertical sun. Results indicate a rapid change for width-to-depth ratios of 1–4 followed by a slower asymptotic change.

1. Introduction

In the real atmosphere, we all recognize that clouds have many different shapes and combinations of length, width and height. Yet, when considering the radiative properties or effects of a cloud, most investigators have treated a cloud as if it were a semi-infinite, horizontally homogeneous medium. One may find examples of the use of this simplification across the entire breadth of the atmospheric sciences; these applications span global energy budget studies (Sellers, 1965; Davis, 1963; London and Sasamori, 1971; Rodgers, 1970; Dopplick, 1972); analytical and numerical modeling of atmospheric motions (Arakawa *et al.*, 1974; Manabe, 1969; Oliger *et al.*, 1970; Sasamori, 1968); and remote sensing of atmospheric variables from satellites (Rodgers, 1970). Indeed, this assumption invades virtually every niche of atmospheric science where radiation computations are used.

In a previous paper (McKee and Cox, 1974; hereafter MC) we contested the virtually universal application of the infinite cloud assumption. In the 1974 paper we addressed the potential impact of the finite horizontal extent cloud on irradiance values. In an independent investigation, Busygin *et al.* (1973) studied the scattering diagram and the albedo of a single cumulus cloud; they also examined the effect of changing the finite cloud shape. Both of the aforementioned investigations concluded that there were very significant differences between calculated irradiance fields using the semi-infinite and the finite cloud assumption.

It is the purpose of this paper to present calculated radiance patterns for a finite cubic cloud. From these radiance data, one may better evaluate the impact of the infinite cloud assumption on specific applications where shortwave radiance values may be used.

2. Monte Carlo computation

The Monte Carlo method has been described in detail by Cashwell and Everett (1959). Several investigations, including those by Kattawar and Plass (1971) and Danielson *et al.* (1969), have used the method to calculate scattering in semi-infinite horizontal cloud layers. Busygin *et al.* (1973) and MC have examined scattering in finite-shaped clouds using the Monte Carlo method. Details of the method used in the present paper were reported by MC.

The use of the Monte Carlo technique to calculate the transfer of radiation in clouds is essentially a direct simulation of the physical process affecting the radiation. A set of boundaries is defined for the geometrical limits of the cloud. Photons from the source are then introduced into the cloud region traveling in a specified direction and the distance the photon travels until an interaction occurs is determined. Then the type of interaction, namely, scattering or absorption, is determined. If scattering occurs, then the new direction of travel after the scatter is selected from the appropriate phase function. These processes are repeated until the photon is absorbed or escapes through a boundary. When large optical depths are used and computer time becomes

prohibitive, photons are assigned a weight which is allowed to escape in fractions of the actual photon energy. Photons are then forced to have collisions until their entire energy has escaped, such that the same answer is obtained as though direct simulation had been pursued.

The present simulation is for an isolated cloud which has no absorption. No atmosphere exists outside the cloud and the ground absorbs all radiation which is incident on it. Consequently, the only processes simulated are the distance traveled between interactions and the change in direction caused by the interaction. The assumption of an absorbing ground is most valid for an ocean surface.

For the present computation, the volume scattering coefficient and phase function have been obtained from Deirmendjian (1969) for a water cloud C.1 and wavelength of 0.45 μm. The cloud was comprised of water droplets with a size distribution given by

$$n = 2.373\, r^6 \exp(-1.5r),$$

which is a model for a cumulus cloud where n represents the number of droplets cm^{-3} for a given radius r. For a value of n of 100 cm^{-3}, the volume scattering coefficient is 16.33 km^{-1} and the liquid content 0.063 g m^{-3}. The relationship between optical depth and geometric depth is linear and is determined by the liquid water content. A geometric depth of 1 km corresponds to an optical depth of 16.33 for a liquid water content of 0.063 g m^{-3}. For a liquid water content of 0.2 g m^{-3}, a 1 km thickness becomes an optical depth of 51.8. The phase function is characterized by a very strong forward scattering peak. The probability of scattering between 0 and α is shown in Fig. 1. Fifty percent of the radiation is contained within the first 6° of the forward direction.

A sketch of a cubic cloud with the coordinate system used in the computations is shown in Fig. 2. Incident sunlight is always in the (y,z) plane which restricts direct sunlight to the top and xy face of the cube. The two angles used to specify exiting radiation are zenith angle θ measured from the Z axis and an azimuth ϕ measured from the $-y$ axis. A ϕ value

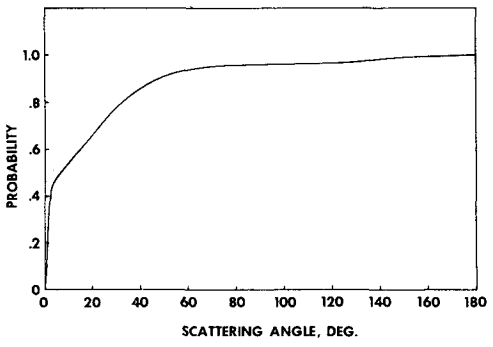

FIG. 1. Cumulative probability of photon scatter as a function of scattering angle.

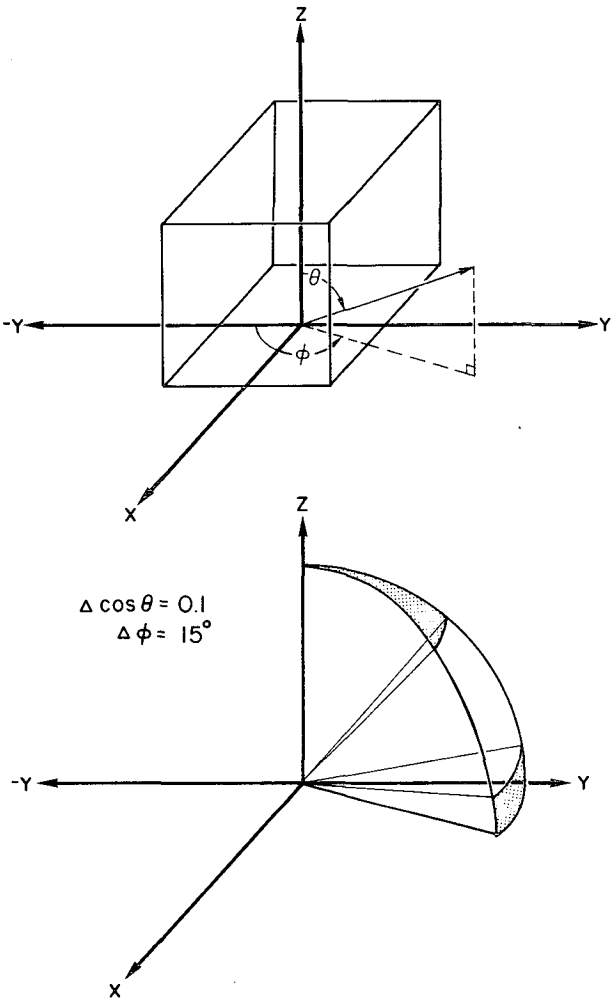

FIG. 2. Cubic cloud with coordinate system and solid angles for relative radiance.

of zero is away from the sun and a value of π is toward the sun. Relative radiance values shown in subsequent graphs are averaged over a finite solid angle. The solid angle used is

$$\Delta\omega = \Delta \cos\theta \Delta\phi,$$

where $\Delta \cos\theta = 0.1$ and $\Delta\phi = 15°$. Radiances shown are relative to a solar irradiance of π. Consequently, a diffuse reflecting surface of unity albedo would be characterized by a relative radiance of unity in all directions.

An example of a solid angle near vertical and near horizontal is shown in Fig. 2. The solid angle near zenith is characterized by a much larger span of zenith angle than the solid angle near horizontal. Radiances exiting the top and sides are computed for identical solid angles so that direct addition of radiances is possible. However, the inherent symmetry of the cube is not exact in the graphs, since radiation leaving the cube perpendicular to the top or per-

pendicular to one face is determined by averaging over solid angles of the same magnitude but, due to the choice of the coordinate system, of different shapes.

The accuracy of the present computation is illustrated in Fig. 13, where the vertical bars denote one standard deviation above and below the calculated values. Computations for a limited range (15°) of azimuth angles, as shown presented in several of the figures, have standard deviations about a factor of 3.3 greater than those shown in Fig. 13. An exception is the case of solar zenith of zero when relative radiances from the top have an accuracy similar to that given in Fig. 13.

3. Radiance from clouds

Radiance characteristics of finite cubic clouds are strongly influenced by radiant energy exiting the sides of the clouds. The present computations represent averaging over a complete face of the cube and over a finite solid angle. To allow direct addition of radiances from the top and sides, the averaging over a solid angle must be constrained to an identical geometry for each face. The geometry selected uses a zenith angle measured from the vertical and an azimuth measured as a rotation about the vertical.

A comparison of radiances from a semi-infinite cloud layer and the top of a cube are shown in Fig. 3 as a function of cloud thickness for a solar zenith (θ_0) of 0°. Optical thickness is equivalent to geometric thickness but varies linearly with liquid water content for a specified distribution of droplets. Fig. 3 illustrates two zenith angles, one near vertical, $\cos\theta = 1.0$–0.95, and one near 60°, $\cos\theta = 0.55$–0.50. The semi-infinite cloud layer radiance increases very rapidly for optical thickness from 5 to 20. Radiance values greater than 1.0 for $\cos\theta = 1.0$–0.95 are more than 90% of the theoretical maximum for thick clouds. Consequently, the radiance values for the semi-infinite cloud layer will change little as the cloud grows in thickness beyond a value of 73.5. The radiance from the cubic cloud increases more slowly with cloud thickness since energy escapes out through the sides of the cloud. For an optical thickness of 73.5, the radiances from the cubic cloud are only slightly greater than one-half the radiances from the semi-infinite cloud layer. The radiance from the cube must increase more than that from the semi-infinite layer as optical depth increases beyond 73.5, since the maximum value for a very large cube will be nearly the same as the semi-infinite layer. However, for a large range of optical thickness and a solar zenith of zero, the radiance from the cube top is significantly smaller than for the semi-infinite cloud.

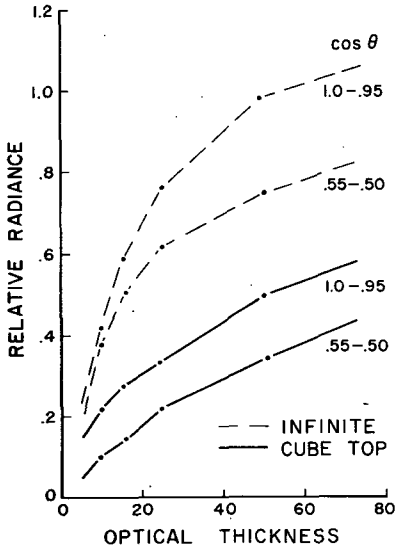

FIG. 3. Relative radiance as a function of optical thickness of $\theta_0 = 0°$.

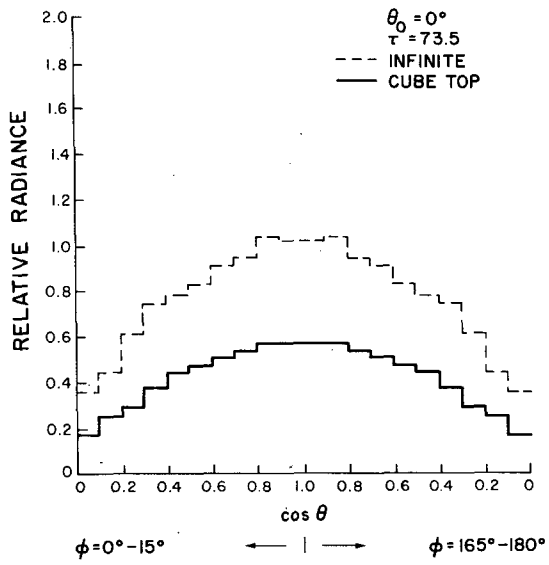

FIG. 4. Relative radiance in the solar plane for an optical depth of 73.5 and solar zenith angle $\theta_0 = 0°$.

Solar radiation enters both the top and one face of the cube for solar zenith angles other than zero. Since the cube then receives more radiation than an equivalent area of the infinite cloud, important changes are possible for the radiances leaving the cloud. Scans of radiance in the solar plane (y,z) for $\theta_0 = 0°$, $\theta_0 = 30°$ and $\theta_0 = 60°$ are presented in Figs. 4, 5 and 6, respectively. When the sun is vertical, the maximum radiance is also vertical and diminishes as the viewing zenith angle increases. Radiance for the infinite cloud is uniformly larger than for the cube. Changes are not dramatic as the solar zenith is moved to 30°, even though the cube does receive about 37% of its energy through a side. Radiation has a shorter path to scatter and emerge in the azimuth away from the sun, and it is evident for both types of clouds. An incident solar zenith of 60° produces startling changes. A strong

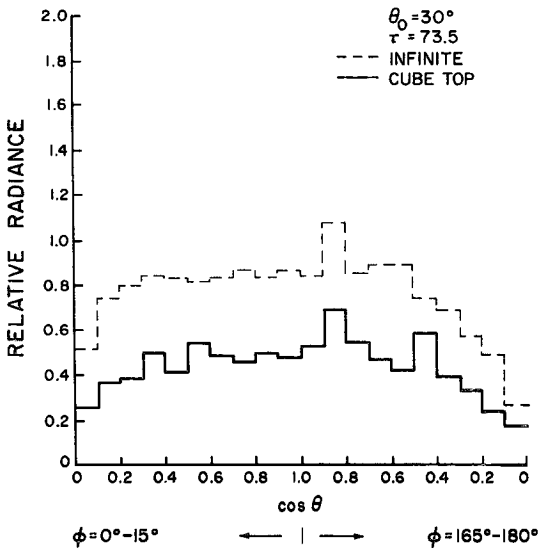

FIG. 5. As in Fig. 4 except for $\theta_0=30°$.

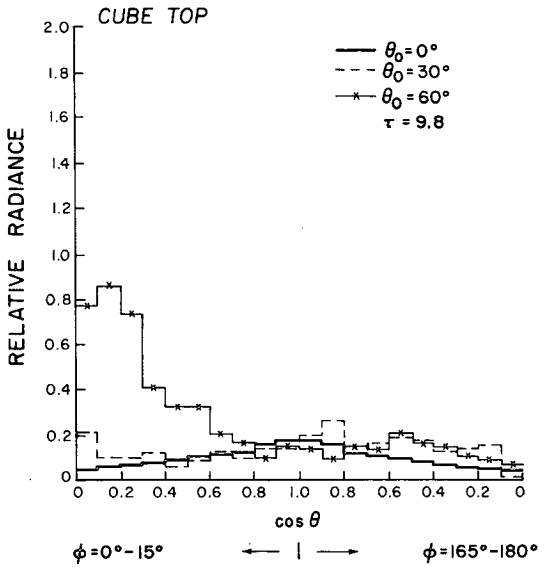

FIG. 7. Relative radiance in the solar plane from the cube top for an optical depth of 9.8.

scattering peak in radiance at large zenith angles is produced for the semi-infinite cloud for $\phi=0°$–15°. However, the radiance from the cube which was much smaller than the infinite cloud for $\theta_0=0°$ and 30° is now nearly the same and the curves are similar. Energetically, the cube is receiving nearly 63° of the energy entering the side toward the sun.

The line on Fig. 6 labeled cube top and side is the radiance which would be viewed by a satellite instrument with a field of view large enough to contain the whole cloud but not able to distinguish the top from the side. The instrument would respond only to the cloud top looking vertically down but would receive a mixture of top and side with less from the top and more from the side as zenith angle increased. The limit near horizontal would be essentially determined by the side. As a result a scan by such an instrument would not detect the strong radiance peak in Fig. 6. In fact, a minimum occurs near horizontal due to the contribution from the side which was not directly illuminated. This is an example of why great care is needed in the interpretation of satellite-observed radiances when small clouds are involved.

Radiance exiting a small cubic cloud with an optical depth of 9.8 is illustrated in Figs. 7–9. Radiance is shown in the solar plane from the top (Fig. 7), the solar face (Fig. 8) and the antisolar face (Fig. 9). Solar zenith angles of 0°, 30° and 60° are included in each graph.

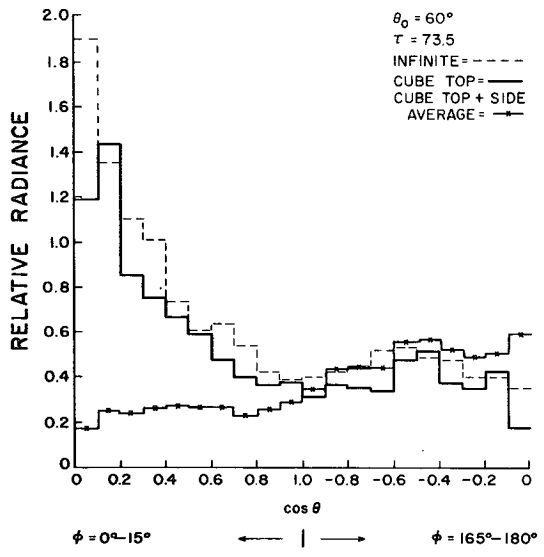

FIG. 6. As in Fig. 4 except for $\theta_0=60°$.

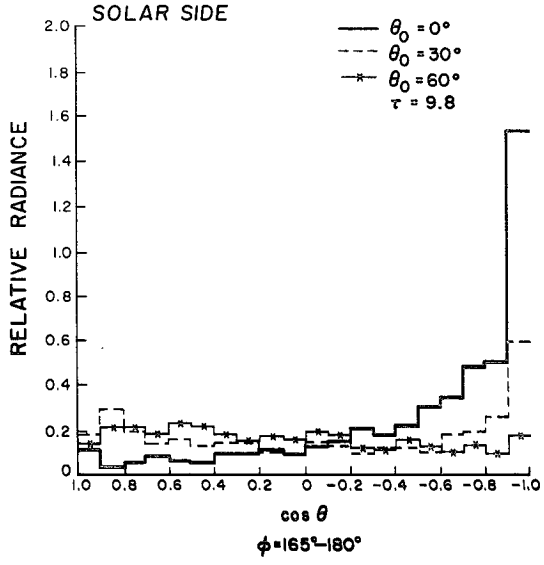

FIG. 8. As in Fig. 7 except from the cube solar side.

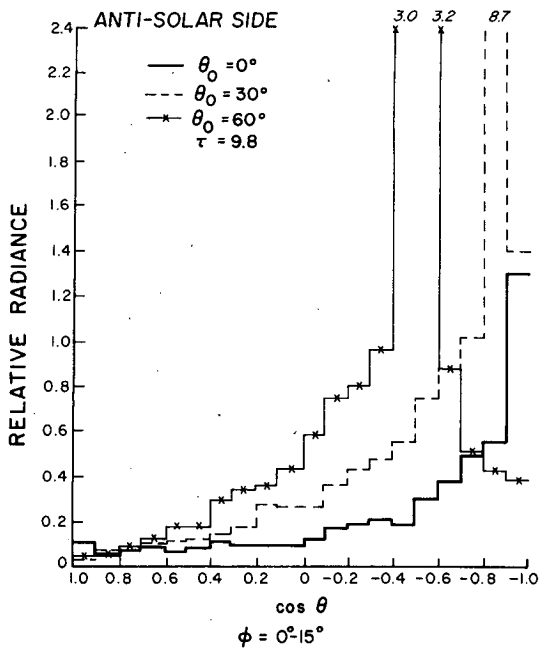

FIG. 9. As in Fig. 7 except from the cube antisolar side.

When the sun is vertical, only 0.005% of the light is not scattered by the cloud. For $\theta_0=0°$, strong forward scattering is evident as light escapes the sides with only small angular changes from the incident light and produces a maximum radiance near $\cos\theta=-1.0$ in Figs. 8 and 9. The maximum from the sides is actually larger than the maximum scattered out of the bottom. Radiance from the sides diminishes to less than 0.12 for upward directions. The top shows the characteristic radiance maximum in the vertical direction.

For solar zenith of 30°, a total of 36.7% more light strikes the cube than for the vertical condition. However, 6.7% of the incident light passes through the cube near the edges with no interaction and exits at $\cos\theta=-0.866$. The radiance contributed by the unscattered light is not included in the graphs. The radiance due to scattering along small optical paths near the edges produces a large peak in Fig. 9 of 8.7. Nearly all light emerging in the large peak entered the cloud top. At $\theta_0=30°$ the incident light is actually 60° away from the normal to the solar side and the radiance from the solar side exhibits a maximum of about 0.6 near $\theta=-1.0$.

For a solar zenith of 60° the total energy striking the cube is the same as for 30°, but the role of the top and solar side are reversed. Again 6.7% of the light passes through the cube with no interaction and exits at $\cos\theta=-0.500$. Scattered radiation which leaves the antisolar side (Fig. 9) near $\cos\theta=-0.500$ is spread into two solid angle domains, and radiances then appear smaller than for the $\theta=30°$ condition. The radiance from the top exhibits a maximum in the forward direction near $\cos\theta=0.0$ due to the shorter path which photons can follow to exit the cloud. The radiance from the top for $\theta_0=60°$ is identical by symmetry to the radiance from the solar side for $\theta_0=30°$. The major difference in appearance is the shape of the solid angle which is represented in each figure.

Several changes occur in the scattered radiance field as the cloud becomes optically thicker. Figs. 10, 11 and 12 contain the radiances from the top, solar side and antisolar side for a cloud with optical thickness of 73.5. Two important changes are that less light is scattered through the cloud and more light exits the face which the light entered. The radiance for $\theta_0=0$

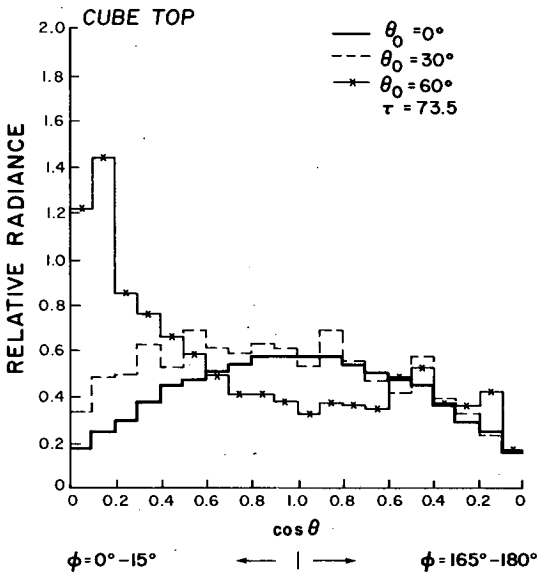

FIG. 10. Relative radiance in the solar plane from the cube top for an optical depth of 73.5.

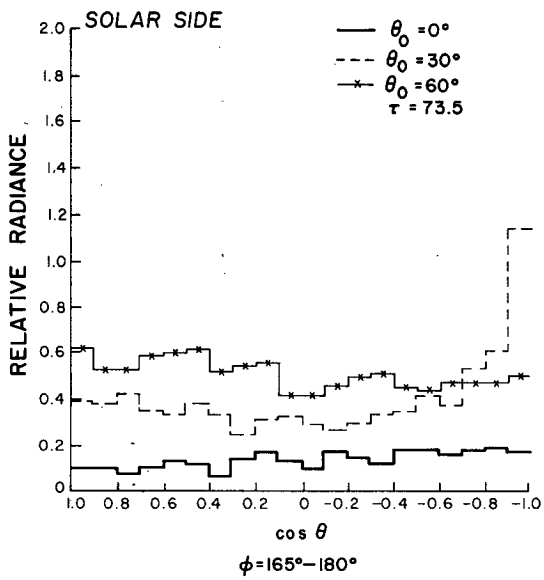

FIG. 11. As in Fig. 10 except from the cube solar side.

indicates larger radiance for the top (Fig. 10), smaller radiance from the sides, and the large downward radiance for the sides is reduced to only a slight increase when averaged over the side of the thicker cloud. At $\theta_0 = 30°$ and $\theta_0 = 60°$, the radiance from the antisolar face is reduced and the peak is likewise strongly diminished. The radiance peaks forward from the top for $\theta_0 = 60°$ are evident.

A transition from a cubic cloud to a semi-infinite layer cloud is easily accomplished by fixing the depth of the cloud and allowing the sides to expand horizontally. Radiances from the top of such a cloud are shown in Fig. 13 for the condition of a solar zenith angle of zero and a vertical optical depth of 73.5. Three emergent zenith angles are included for a width-to-depth ratio from 0.33 to 12. The relative radiance rises rapidly up to a ratio of about 4 and then proceeds to an asymptotic type approach toward the semi-infinite layer radiance.

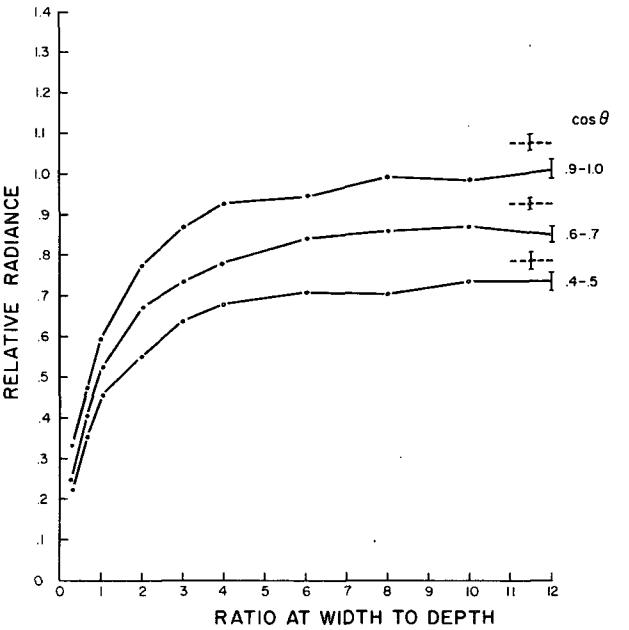

FIG. 13. Relative radiance from cloud top for solar zenith of 0.0° as a function of the width-to-depth ratio. See text (Section 2) for a discussion of computation accuracy represented by the one standard deviation vertical bars.

4. Implications

The differences between semi-infinite and finite clouds illustrated by this paper and by Busygin *et al.* (1973) may very well have a significant effect on several areas of atmospheric research. The most obvious area affected by these differences is that of satellite observations of the earth's atmosphere and surface. Bi-directional reflectance of satellite-observed shortwave radiances will be different in principle for small clouds and layer clouds. The differences will affect not only interpretation of raw data, but also the application of data to energy budget studies. Another area of impact is the satellite brightness and cloud-height correlation reported by Griffith and Woodly (1973). The finite-to-infinite cloud radiance differences for a vertical sun condition offer the most promising explanation for the observed increase of brightness with cloud height, i.e., the observed increase of brightness is due to the increase in horizontal size of the cloud.

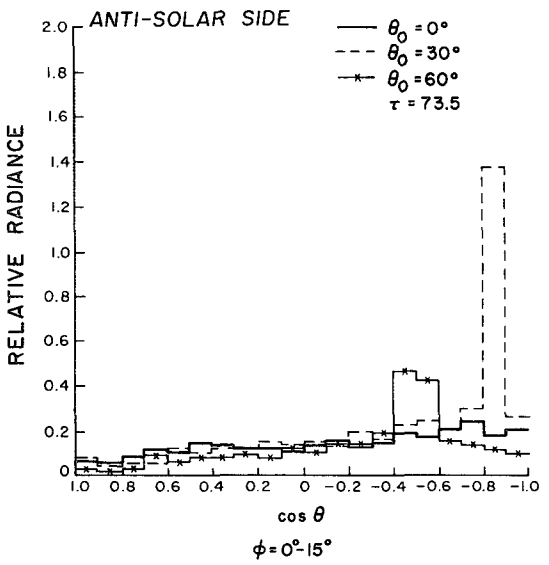

FIG. 12. As in Fig. 10 except from the cube antisolar side.

Satellite observations of surface characteristics are often dependent on subtracting out the effects of small clouds. A valid interpretation relies upon an understanding of the effects of small clouds on upward and downward radiances. Finite-to-infinite cloud radiance differences are also effective in developing an understanding of global and regional surface energy budgets. Indeed it may be desirable to monitor cloud-size distributions from satellites in order to establish representative global and regional albedo variations.

Parameterization of radiation flux divergences and surface radiation budgets in large-scale dynamical models of atmospheric motions have been based on the infinite cloud assumption. The results of MC, this paper and Busygin *et al.* (1973) suggest that such a model could not be expected to produce correct cloud amount, surface radiation budget and planetary radiation budget at the same time. Whether or not an additional degree of freedom, cloud-size spectrum, should be considered in the determination of the radiation budget in these models is certainly an appropriate question. The evidence offered by the aforementioned authors is sufficiently convincing to conclude that the effects of finite clouds must be included, either implicitly or explicitly, in atmospheric models of virtually all time and space scales. Since the radiation budgets act as strong, if not dominant, forcing

functions in most dynamic and thermodynamic models, it is especially important that the cloud amount/radiation budget relationship be thoroughly understood and accounted for. It is not suggested that a Monte Carlo radiation computation be included in a general circulation model, but that the radiation parameterization take into account the differences in radiative characteristics between finite and infinite clouds.

5. Concluding remarks

Calculated distributions of scattered shortwave radiance have been presented for approximate simulated cumulus clouds using a cubic shape. A comparison with similar clouds of semi-infinite horizontal extent has been included. For an incident solar zenith angle of 0°, the angular distribution of the radiance exiting cloud top is similar for the cube and the semi-infinite layer, but the radiance is much smaller for the cube for optical depths up to 73.5. At optical depth 73.5 the vertical radiance from the cube is only 58% of that from the semi-infinite layer cloud. For an incident solar zenith angle of 60°, the angular distribution and the magnitude of the scattered radiance in the solar plane are very much alike. Radiances exciting the antisolar side of the cloud illustrate the strong forward scattering for short optical paths near cloud edges which is still evident at optical depth 73.5.

The transition from cubic clouds to semi-infinite layers was illustrated for a vertical sun. Results indicate a rapid change for width-to-depth ratios of 1–4, followed by a slower asymptotic change which is not complete for a width-to-depth ratio of 12.

Acknowledgments. This research was supported by the Global Atmospheric Research Program, Office of Climate Dynamics, National Science Foundation and the GATE Project Office, National Oceanic and Atmospheric Administration. Computer time was provided by the National Center for Atmospheric Research which is sponsored by the National Science Foundation.

REFERENCES

Arakawa, A., A. Mintz and collaborators, 1974: The UCLA atmospheric general circulation model. Dept. of Meteorology, UCLA, Los Angeles. [Available from the author at the Dept. of Meteorology, University of California, 405 Hilgaard Avenue, Los Angeles.]

Busygin, V. P., N. A. Yevstratov and Ye. M. Feygel'son, 1973: Optical properties of cumulus and radiant fluxes for cumulus cloud cover. *Atmos. Oceanic Phys.*, **9**, 1142–1151.

Cashwell, E. D., and C. J. Everett, 1959: *A Practical Manual on the Monte Carlo Method for Random Walk Problems.* Pergamon Press, 153 pp.

Danielson, R. E., D. R. Moore and H. C. Van de Hulst, 1969: The transfer of visible radiation through clouds. *J. Atmos. Sci.*, **26**, 1078–1087.

Davis, Paul A., 1963: An analysis of the atmospheric heat budget. *J. Atmos. Sci.*, **20**, 5–22.

Deirmendjian, D., 1969: *Electromagnetic Scattering on Spherical Polydispersions.* American Elsevier, 290 pp.

Dopplick, T. G., 1972: Radiative heating of the global atmosphere. *J. Atmos. Sci.*, **29**, 1278–1294.

Griffith, Cecila G., and William L. Woodley, 1973: On the variation with height of the top brightness of precipitating convective clouds. *J. Appl. Meteor.*, **12**, 1086–1089.

Kattawar, G. W., and G. N. Plass, 1971: Radiance and polarization of light reflected from optically thick clouds. *Appl. Opt.*, **10**, 74–80.

London, J., and T. Sasamori, 1971: Radiative Energy Budget of the Atmosphere. *Space Research XI*, Akademie-Verlag, Berlin, 639–649.

Manabe, Syukuro, 1969: Climate and ocean circulation. I. The atmospheric circulation and the hydrology of the earth's surface. II. The atmospheric circulation and the effect of heat transfer by ocean currents. *Mon. Wea. Rev.*, **97**, No. 11.

McKee, T. B., and S. K. Cox, 1974: Scattering of visible radiation by finite clouds. *J. Atmos. Sci.*, **31**, 1885–1892.

Oliger, J., R. Wellck, A. Kasahara and W. Washington, 1970: Description of NCAR Global Circulation Model. National Center for Atmospheric Research, Boulder, Colo. [Available from Publications Dept., NCAR].

Rodgers, C. D., 1970: Remote sounding of the atmospheric temperature profile in the presence of cloud. *Quart. J. Roy. Meteor.*, **96**, 654–666.

Sasamori, Takashi, 1968: The radiative cooling calculation for application to general circulation experiments. *J. Appl. Meteor.*, **7**, 721–729.

Sellers, William D., 1965: *Physical Climatology.* The University of Chicago Press, 272 pp.